Analyst

Cite this: *Analyst*, 2012, **137**, 2176

www.rsc.org/analyst

PAPER

Magnetic beads-based electrochemiluminescence immunosensor for determination of cancer markers using quantum dot functionalized PtRu alloys as labels†

Yan Zhang,[a] Shenguang Ge,[ab] Shaowei Wang,[a] Mei Yan,[a] Jinghua Yu,*[a] Xianrang Song*[c] and Weiyan Liu[a]

Received 29th November 2011, Accepted 18th February 2012
DOI: 10.1039/c2an16170b

A novel electrochemiluminescence (ECL) immunosensor for sensitive detection of human chorionic gonadotrophin antigen (HCG-Ag) was constructed using CdTe quantum dot functionalized nanoporous PtRu alloys (QDs@PtRu) as labels for signal amplification. In this paper, nanoporous PtRu alloy was employed as the carrier for immobilization of CdTe QDs and antibodies. Primary monoclonal antibody to alfa-HCG antigen ($McAb_1$) was immobilized onto the surface of chitosan coated Fe_3O_4 magnetic nanoparticles (Fe_3O_4/CS MNPs) by glutaraldehyde (GA) as coupling agent. Then $McAb_1$ could be easily separated and assembled on the surface of indium tin oxide glass (ITO) owing to their excellent magnetic properties with external magnetic forces holding the MNPs. Due to signal amplification from the high loading of CdTe QDs, 4.67-fold enhancements in ECL signal for HCG-Ag detection was achieved compared to the unamplified method (single QDs as labels). Under optimal conditions, a wide detection range (0.005∼50 ng mL^{-1}) and low detection limit (0.8 pg mL^{-1}) were achieved through the sandwich-type immunosensor. The novel immunosensor showed high sensitivity and selectivity, excellent stability, and good reproducibility, and thus has great potential for clinical detection of HCG-Ag. In particular, this approach presents a novel class of combining bifunctional nanomaterials with preferable ECL properties and excellent magnetism, which suggests considerable potential in a wide range of applications for bioassays.

1. Introduction

During recent years, nanomaterials and nanotechnology have been extensively studied because of their great potential in disease diagnosis and therapy.[1–3] A broad range of nanoscale inorganic particles including MNPs and QDs have been systematically investigated for their unique physical and chemical properties, and their potential applications in bio-detection, molecular imaging, and photothermal therapy of tumors.[4–8] For instance, functionalized MNPs with different groups, which have the special properties of aggregating and separating through a magnet, have been used as special biomolecule immobilizing carriers with good biocompatibility, and have provided an alternative immobilization method for the construction of immunosensors. Successful applications of MNPs in the immobilization of biomolecules have also been reported.[9–11] The functionalized MNPs offer the following advantages: (1) more specific surface area for binding larger amounts of biomolecules can be obtained;[12] (2) selective separation of the immobilized biomolecules from a reaction mixture on application of a magnetic field can be achieved.[13] In 2007, Li *et al.* developed a renewable potentiometric immunosensor based on Fe_3O_4 nanoparticle immobilized Anti-IgG.[12] Subsequently, Mani *et al.* developed a novel immunosensor using the magnetic beads' high specific surface area to immobilize Ab_2 to amplify sensitivity and to improve the detection limit.[14] Therefore, owing to their attractive properties, MNPs have exhibited a wide application in the field of immunoassays.[15] QDs have also recently received tremendous attention due to their possible luminescent applications in aqueous solution.[16] With size-tunable narrow emission spectra and broad excitation spectra, QDs, particularly the modified ones, have been successfully used in immunoassays. For instance, Li *et al.* fabricated graphene-QD composites for sensitive electrogenerated chemiluminescence immunosensing for the detection of IgG,[17] and Yang *et al.* prepared SiO_2-coated QDs to conjugate with IgG.[18]

In the field of nanotechnology, research on combining MNPs with luminescent reagents has been developing rapidly. The possibility of controlling a luminescent reporter or label by

[a]*Key Laboratory of Chemical Sensing & Analysis in Universities of Shandong (University of Jinan), School of Chemistry and Chemical Engineering, University of Jinan, Jinan 250022, China. E-mail: ujn.yujh@gmail.com; Tel: +86-531-82767161*
[b]*Shandong Provincial Key Laboratory of Fluorine Chemistry and Chemical Materials, University of Jinan, Jinan 250022, P.R. China*
[c]*Cancer Research Center, Shandong Tumor Hospital, Jinan 250012, P.R. China. E-mail: sxr@vip.163.com*
† Electronic supplementary information (ESI) available. See DOI: 10.1039/c2an16170b

a magnetic field has attracted the attention of many research groups. Combinations of functioned MNPs and modified QDs have been used to fabricate nanostructures with attractive features such as fluorescence and magnetism,[19,20] and they have provided a new functional platform for biomedical engineering and bioanalytical sciences.

As an important and powerful analytical tool, ECL has recently attracted considerate attention in both fundamental study and analytical applications due to its advantages, such as simplicity, rapidity, high sensitivity, low background signal, easy controllability, and flexibility.[21] However, bioanalysis based on those conventional luminescent reagents possess some limitations. Ruthenium labeling at multiple sites may result in the loss of biological activity of molecules,[22] luminol ECL is weak in neutral solution,[23] and semiconductor nanocrystal ECL shows inferior sensitivity for analytical applications.[24] Therefore, it is necessary to conquer the above luminescent reagent's weakness to develop the ECL applications in bioassays. Modification of the luminescent reagent is a common method to achieve this. Huge efforts have been made towards enhancement of detection sensitivity through signal amplification.

To be used in signal amplification for immunoassays, a delicate balance was required between large loading surfaces to allow more biomolecule loading (*i.e.* increase of the particle size) and small volume to remain suspended in solution and to form immuno-complexes with acceptable diffusion kinetics (decrease of the particle size). The electrochemical immunosensor that utilizes integrating enzyme assisted signal amplification processes, and incorporates nanomaterials to increase loading of tags has been demonstrated to be one of the most practical solutions due to its capability to conduct highly molecular specific measurements.[25–27] Among the nanomaterials used, nanoporous structures have attracted considerable attention due to their promising potential in the use of catalysis,[28] lithium ion batteries,[29] photodynamic therapy[30] and electrical conduction.[31] Owing to their bicontinuous nanoscale skeletons and interconnected hollow channels, they are favorable for easy mass transport and high electron conductivity. Notably, nanoporous PtRu alloy has been extensively studied because of its uniform structural dimensions. The dark skeletal framework confirms the formation of a three-dimensional (3D) interconnected network structure in the nanoscale and the inner bright region represents the bicontinuous hollow channels embedded in the solid nanoarchitectures. With this in mind, nanoporous PtRu alloys can be employed as an ideal carrier to load amounts of other molecules because of their interconnected skeletal framework that is very favorable for electron transport, and the open porous channels extending in all three dimensions facilitate the area-to-volume ratio. Therefore, it is interesting to explore the enhancement of detection sensitivity by an increase of CdTe QDs loading on the surface of nanoporous PtRu alloys. Consequently, CdTe QDs functionalized nanoporous PtRu alloys were selected as labels to develop the sandwich-type immunosensor in this study. To our best knowledge, no immunoassay using ECL of CdTe QDs functionalized nanoporous PtRu alloys has been reported up to the present time.

In this paper, we present a novel strategy that makes use of the promising applications of QDs@PtRu in signal amplification for ultrasensitive detection of cancer biomarkers. Fe_3O_4/CS MNPs and QDs@PtRu were prepared by easy and inexpensive methods and they were combined to fabricate a novel ECL immunosensor. As shown in Scheme 2 later, $McAb_1$ and secondary monoclonal antibody to alfa-HCG antigen ($McAb_2$) were covalently bonded to Fe_3O_4/CS MNPs and QDs@PtRu, respectively. To make use of the magnetic properties of the immunosensor, a flow injection (FI) ECL detecting cell using ITO as working electrode (WE) was fabricated. The immunosensor was highly sensitive and selective, and exhibited excellent stability and good reproducibility. Thus, it has great potential for clinical protein detection. Moreover, this work would open up a new field in ECL application of nanoporous material to load more labels for highly sensitive bioassays.

2. Materials and methods

2.1. Reagents

All reagents were of analytical-reagent grade or the highest purity available and directly used for the following experiments without further purification and the aqueous solutions unless indicated were prepared with doubly distilled water. ITO (thickness of ITO layer: 150 nm; resistance < 15 Ω/square; thickness of glass: 1.1 mm) was obtained from Xiamen ITO Photoelectricity Industry (Xiamen China). HCG-Ag, $McAb_1$ and $McAb_2$ were purchased from Shanghai Linc-Bio Science Co. Ltd (Shanghai, China), and the standard HCG-Ag, primary monoclonal antibody to alfa-HCG antigen ($McAb_1$), $McAb_2$ stock solutions were prepared with phosphate-buffered saline (PBS, pH 7.4, 10 mM) and stored at 4 °C. Glutaraldehyde solution (GA, 25%), chitosan (CS, 85% deacetylation), disodium hydrogen phosphate (Na_2HPO_4), sodium dihydrogen phosphate (NaH_2PO_4), ferric chloride ($FeCl_3$), ferrous chloride ($FeCl_2 \cdot 4H_2O$) and sodium hydroxide (NaOH) were obtained from Sinopfarm Chemical Reagent Co., Ltd (Shanghai, China). Bovine serum albumin (BSA) was bought from Shanghai Boao Bio-Technology Co., Ltd (Shanghai, China). Thioglycolic acid (TGA), *N*-(3-dimethylaminopropyl)-*N*′-ethylcarbodiimide hydrochloride (EDC) and *N*-hydroxysuccinimide (NHS) were purchased from Alfa Aesar China Ltd. Tellurium (Te) powder, sodium borohydride ($NaBH_4$), cadmium chloride ($CdCl_2 \cdot 2.5H_2O$), and $Cd(ClO_4)_2$ were supplied by Shanghai Chemical Reagent Company (Shanghai, China). The washing buffer was PBS (0.01 M, pH 7.4), 0.01 M PBS of various pH, prepared by adjusting the ratio of Na_2HPO_4 to NaH_2PO_4 containing 0.1 M $K_2S_2O_8$, was used as the electrolyte in the measuring system. The clinical serum samples were provided by Shandong Tumor Hospital.

2.2. Apparatus

The ECL experiments were carried out on a MPI-B multiple-parameter chemiluminescence analytical testing system equipped with a MPI-A/B multifunction chemiluminescence detector (Xi'An Remax Electronic Science & Technology Co. Ltd. Xi'an, Changchun Institute of Applied Chemistry Chinese Acamedy Sciences, China) at room temperature. The PL spectra were obtained on a LS-55 spectrofluorometer (P.E. USA). UV-vis

absorption spectra were recorded on a UV-3101 spectrophotometer (Shimadzu, Japan). Thermogravimetric analysis (TG) was conducted under nitrogen atmosphere using STA 490 EP (Netzsch, Switzerland). Infrared spectroscopy (IR) was achieved on a Fourier transform infrared (FT-IR) Spectrum RX (PerkinElmer Spectoment). Scanning electron microscope (SEM) and energy dispersive spectrometer (EDS) images were obtained using a JSM-6700F microscope (Japan). Transmission electron microscope (TEM) images were obtained from a JEOL JEM-1400 microscope (Japan).

2.3. Fabrication of the FI-ECL cell

The FI-ECL cell (Scheme 1) was fabricated using cuboid poly(methylmethacrylate) (PMMA). The ITO slide glass was cut into 1.0 cm i.d. and used as the working electrode. The FI-ECL cell mainly consisted of an ITO working electrode (WE), two flow tubes, a platinum counter electrode (CE), and Ag/AgCl reference electrode (RE). The WE, two flow tubes, CE, and RE were slid together by screws to form the airtight FI-ECL cell. The inlet and outlet were at the slide face of the cell which were nearly at one line with ITO slide glass. At the bottom of the cell, a round optical window was made from which the ECL signal passed from the ITO to the detection system. In addition, there is a vacant space for the magnet at the bottom. The magnet was placed there if needed.

2.4. The synthesis of Fe_3O_4/CS MNPs

The Fe_3O_4/CS MNPs were fabricated *via* a co-precipitation method.[32] In brief, 10 mL of chitosan solution (2 wt%, prepared by dissolving the required amount of chitosan powder in 10 mL acetic acid solution), and 10 mL of $FeCl_3$ (0.1 M) were introduced into a 100 mL round-bottomed flask equipped with a magnetic stirrer. After churning for good distribution, the flask was placed into hot water at 90 °C to reach an homogeneous temperature. N_2 was used to keep purging and produce an aqueous dispersion of magnetic nanoparticles until the end of the synthesis process. Simultaneously, the stirring rate was increased to 3000 rpm, and 5 mL of $FeCl_2$ (0.1 M) were added into the above solution. Maintaining a super-speed of stirring, NaOH (2.0 M) was then slowly added dropwise into the vigorously mechanical-stirred solution until the suspension turned black, the pH values of the solution were about 9–10 at the same time, indicating the formation of minuscule MNPs, which were allowed to remain refluxing to crystallize for another 90 min under magnetic stirring at a constant temperature. After the reaction, the suspension was poured into a beaker which was placed on a permanent magnet, to cool it down to room temperature. The prepared black chitosan-coated Fe_3O_4 MNPs were observed to settle on the bottom of the beaker quickly. The supernatant was discarded and oxygen-free distilled water and ethanol was added to the beaker. This procedure was repeated several times until most of the ions in the suspension had been removed, and the pH of the suspension became less than 7.5. Dry magnetic powders were obtained by drying the residue at 60 °C in vacuum.

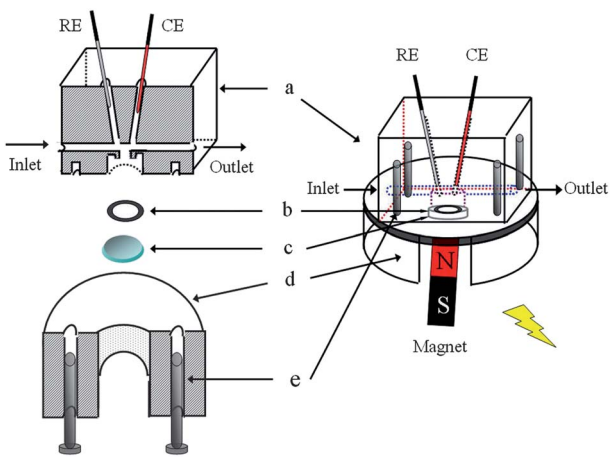

Scheme 1 Schematic diagram of the FI-ECL cell. RE: reference electrode; CE: counter electrode; a: Top perspex block; b: Airtight rubber; c: ITO slide glass; d: Bottom perspex block; e: Screw.

2.5. Preparation of nanoporous PtRu alloys

Nanoporous PtRu alloys used as carrier for CdTe QDs and $McAb_2$ immobilization, were synthesized according to Xu *et al.*'s reported method.[33] Ternary PtRuAl alloy foils were made by refining high-purity (>99.99%) Pt, Ru, and Al at high temperature under the protection of high-purity argon in a furnace, followed by melt-spinning. The structures were obtained after de-alloying PtRuAl alloy for 72 h in 2 mol L^{-1} NaOH solution. Then the nanoporous PtRu alloy was obtained.

2.6. Preparation of water-soluble CdTe QDs and QDs@PtRu

The water-soluble CdTe QDs were synthesized using TGA as stabilizing agent according to a similar method reported previously.[34] Briefly, 0.1980 g of $CdCl_2 \cdot 2.5H_2O$ was dissolved in 50 mL of water, then 160 μL of TGA added. The pH of the solution was adjusted to 10 by 1.0 M NaOH solution. The resulting clear solution was bubbled with high purity N_2 for 30 min, and 10.0 mL of the NaHTe solution (produced by the reaction of 0.1190 g $NaBH_4$ and 0.0492 g Te powder in oxygen-free water) was injected into the vigorously stirred solution immediately. Different sizes of QDs were obtained by simply varying the refluxing time at 100 °C. The final obtained QD solution was rather stable for more than three months when kept in a refrigerator at 4 °C. The red QDs with particle size about 7 nm (Fig. 1A) were selected for the next step.

For the preparation of QDs@PtRu, 0.5 mg nanoporous PtRu alloy was first dispersed in 1 mL of PBS (pH 7.4) by sonication. Then, 1.00 mL of prepared CdTe QDs was added into the solution. The mixture was allowed to react at room temperature under stirring for 4 h, followed by centrifugation of TGA stabilized CdTe QDs that could be loaded into the nanoporous PtRu alloy.[35,36] Unbound QDs were removed by successive centrifugation and washing with water several times. Finally, the as-prepared QDs@PtRu, which had the same orange color as CdTe QDs itself, was obtained and dispersed in water to a final volume of 1.00 mL. The solution was stored at 4 °C for further use.

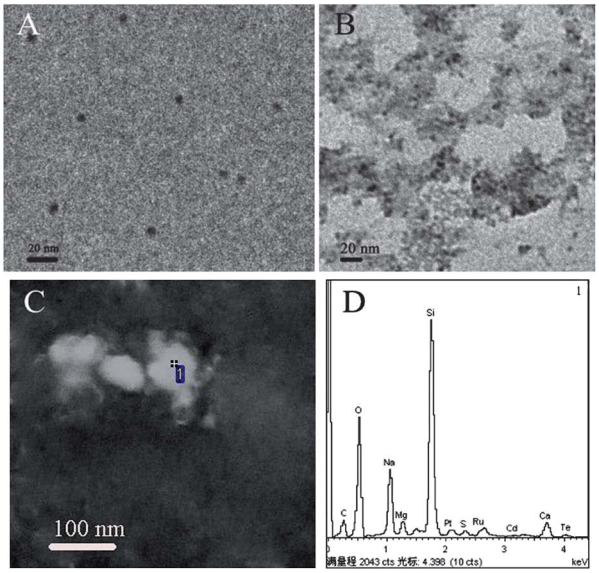

Fig. 1 TEM of CdTe QDs (A), QDs@PtRu (B), SEM of QDs@PtRu (C) and EDS of QDs@PtRu (D).

2.7. Fabrication of the ECL immunosensor

The schematic diagram of preparation of the ECL immunosensor is shown in Scheme 2. Firstly, the synthesized Fe_3O_4/CS MNPs were washed by PBS (0.01 M, pH 7.4) and collected with the help of a magnetic plate. Secondly, 50 μL of GA (2.5%) was added into the freshly washed Fe_3O_4/CS MNPs solution (2 mg mL^{-1}) and allowed to react for 1.0 h at room temperature. It acts as a bridge to connect Fe_3O_4/CS MNPs with $McAb_1$. To remove any unconjugated materials, several washes with PBS buffer were carried out by using a permanent magnet. Finally, the Fe_3O_4/CS-GA conjugate was re-dispersed in PBS and stored at 4 °C for further characterization.

$McAb_1$ (10 μL, 20 μg mL^{-1}) together with PBS (20 μL) were added into the above mixture to react for 60 min at 4 °C. To remove any unbound antibody, the mentioned solutions were rinsed using a permanent magnet. Subsequently, 50 μL of BSA (1 wt %) was added into the Fe_3O_4/CS-GA-$McAb_1$ solution to react for 1.0 h to block the nonspecific binding sites on the surface of Fe_3O_4/CS MNPs. After washing, the immunosensor was re-dispersed in PBS and stored at 4 °C for further usage.

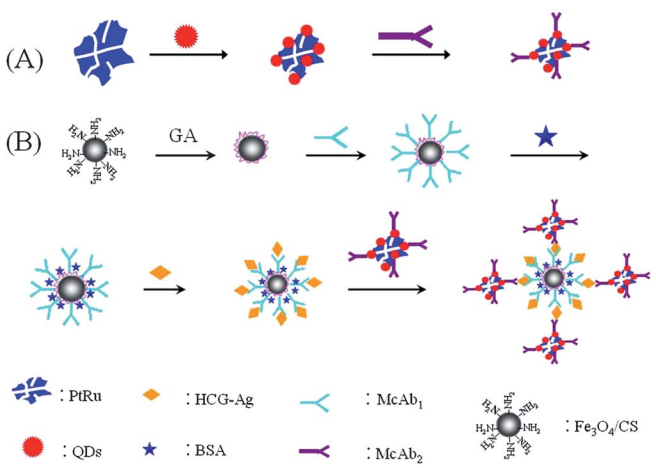

Scheme 2 Schematic representation of the fabrication of the ECL immunosensor.

2.8. ECL detection of HCG-Ag with the immunosensor

At first, the immunosensor was incubated with different concentrations of HCG-Ag solution for 50 min at 4 °C. After that the HCG-Ag was immobilized on the surface of Fe_3O_4/CS-GA-$McAb_1$. In order to wipe out the unconjugated antigen, the modified Fe_3O_4/CS-GA-$McAb_1$ were rinsed once more, and re-dispersed in PBS. Subsequently, QDs@PtRu labeled $McAb_2$ conjugation (prepared by mixing QDs@PtRu, EDC, NHS, $McAb_2$) was added into the mentioned solutions and incubated for 55 min at 4 °C. With the help of a magnet, the unbound QDs@PtRu labeled $McAb_2$ were washed out. After that, the prepared ECL immunosensor was dispersed in PBS containing 0.1 M $K_2S_2O_8$, and conveyed into the homemade detecting cell by a FI system, and assembled on the surface of the ITO WE with the help of a magnet, in contact with PBS. Subsequently, the magnet was carefully taken away to avoid the movement of Fe_3O_4/CS MNPs, and the cell was placed on the top of the PMT. Ultimately, the ECL immunosensor was applied to detect HCG-Ag.

3. Results and discussion

3.1. Improvement of the FI-ECL cell

Compared with the conventional FI cells, the homemade FI-ECL cell has some apparent advantages.

(i) The inlet, outlet, and ITO slide glass were nearly at the same horizontal line. The diameter of inlet and outlet were 1.0 mm. So this kind of ECL detector has a relative small dead volume.

(ii) The ITO WE was placed opposite the transparent window, resulting in nearly 100% of the luminescence emission generated at the surface of the WE, which could be captured by PMT. The design surmounted the weakness of the ECL emission scattered in all directions.

(iii) The ITO WE, situated at the bottom of the detector, could be replaced by another one by handling the screws before its service life. Compared with the glassy carbon electrode or gold electrode, the ITO slide glass was cost-effective and was used for high-quantity production.

What's more, the ITO slide glass was cut into 1.0 cm i.d. The area was larger than that of the glassy carbon electrode or gold electrode, which makes the ECL detector have a high sensitivity.

3.2. Characterization of Fe_3O_4/CS MNPs

(i) FT-IR analysis. FT-IR analysis was performed to characterize the surface character of Fe_3O_4 and Fe_3O_4/CS MNPs. As shown in the ESI (Fig. S1†), the strong absorbing peaks at 586 cm^{-1} and 3420 cm^{-1} (curve a) are on behalf of the bind of Fe–O, and –OH group on the Fe_3O_4 MNPs surface, respectively. Compared with that, the characteristic band at 3420 cm^{-1} of curve b corresponded to the stretching vibration of the $–NH_2$ group and –OH group, and the characteristic band at 1069 cm^{-1} represented the presence of the –C–O– group of chitosan. The

absorption band at 1642 cm^{-1} was assigned to the "free" amino group of chitosan. Furthermore, the red shift of the absorbing of Fe–O presented at 538 cm^{-1}, and the peak shape has changed slightly compared with that in Fig. S1a.† Because of the linkage of Fe_3O_4 with CS, CS has been polymerized to composite nanoparticles.

(ii) Thermogravimetric analysis (TG). In the interval of 60–100 °C, the weight-loss percentage of Fe_3O_4 and Fe_3O_4/CS was approximately 7.5% (Fig. S2†), which corresponded to the evaporation of H_2O. Compared with curve a, the weight-loss percentage was nearly 26.5% with an apparent decline between 250 °C and 400 °C on curve b, which is assigned to the chemical interactions between the Fe_3O_4 nanoparticles and chitosan. It is possible that these interactions increased the decomposition temperature of the chitosan coated on the Fe_3O_4 nanoparticles. Beyond 550 °C, there is hardly any change in mass, which means that the remainder was pure Fe_3O_4 MNPs, which is in agreement with Liu's research conclusion.[37]

3.3. Characterization of CdTe QDs and QDs@PtRu

UV-vis and PL spectra were used to characterize the formation of CdTe QDs and QDs@PtRu. As shown in Fig. S3b,† a small red shift of QDs@PtRu PL spectrum was observed compared with that of the CdTe QDs. This phenomenon was ascribed to CdTe QDs bound strongly to PtRu alloy. Moreover, a red shift of absorbtion spectrum was observed (Fig. S3a†), which also could indicate QDs@PtRu had been successfully prepared.

In addition, the preparation of QDs bonding with nanoporous PtRu alloy is illustrated by TEM, SEM and EDS. As shown in Fig. 1B, CdTe QDs (dark dots) are bound strongly with PtRu alloy (light colour), and Fig. 1C–D further confirms the formation of QDs@PtRu. All these results demonstrated that the QDs could be loaded on the surface of nanoporous PtRu alloys. Furthermore, the ECL intensity of QDs@PtRu labeled $McAb_2$ was 4.67-fold higher than that of single QDs labeled $McAb_2$ (Fig. 2) at the same HCG-Ag concentration, which demonstrated the amplification of ECL signal with QDs@PtRu as the label.

3.4. Optimization of experimental conditions

The effects of pH value, applied potential and incubation time on the ECL intensity of the immunosensor were investigated as follows.

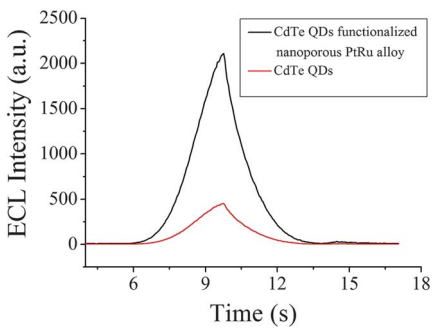

Fig. 2 ECL performance of QDs and QDs@PtRu at one level of HCG-Ag.

The anodic ECL emission of CdTe QDs is depended on the pH value of the detection solution. According to the ECL experimental results (Fig. 3A), PBS (0.01 M, pH 7.6) containing $K_2S_2O_8$ (0.1 M) was selected as the detection solution. QDs@PtRu were used to label the $McAb_2$ to carry out the ECL, hence, the ECL performance of CdTe QDs with HCG-Ag was investigated. Different potentials were investigated, and ECL curves were obtained at eight of them: 0.4–1.4 V (outlined in Fig. 3B). It can be confirmed that the optimal scanning potential was 0.4–1.0 V. Furthermore, the ECL intensity increased as the incubation time increased and then tended to a constant value after some time, which showed a saturated binding between different substances. Therefore, the effect of the incubation time of $McAb_1$ with HCG-Ag (T_1), and HCG-Ag with QDs@PtRu labeled $McAb_2$ (T_2) (Fig. 3C, D) on the ECL intensity of the immunosensor were investigated, which can be seen that the optimal incubation time was 50 min and 55 min, respectively. More or less response time would affect the extent of immunoreaction, resulting in different ECL responses.

3.5. Sensitivity of the immunosensor

Under the optimal conditions, a series of immunosensors was prepared for the detection of different concentrations (c) of HCG-Ag. The ECL intensity response was proportion to the logarithm of the HCG-Ag concentration in the range of 0.005∼50 ng mL^{-1}, the equation of the calibration curve (Fig. 4) was $\Delta ECL = 2199.3 + 1000.5\log c_{HCG\text{-}Ag}$ (ng mL^{-1}), with a correlation coefficient of 0.9945. The limit of detection (LOD) at a signal-to-noise of 3 was 0.8 pg mL^{-1}. The low LOD and large linear range may be attributed to three factors: 1) the intrinsic property of high surface-to-volume ratio of Fe_3O_4/CS, which could greatly increase the loading of $McAb_1$ due to its high surface area; 2) QDs@PtRu with a three-dimensional (3D) interconnected network structure in the nanoscale and the bicontinuous hollow channels embedded in the solid nanoarchitectures can immobilize more QDs to amplify signals; and 3) the good conductivity and electron transfer ability of $S_2O_8^{2-}$ may also help the detection of HCG-Ag, making the detection limit lower and the linear range larger.

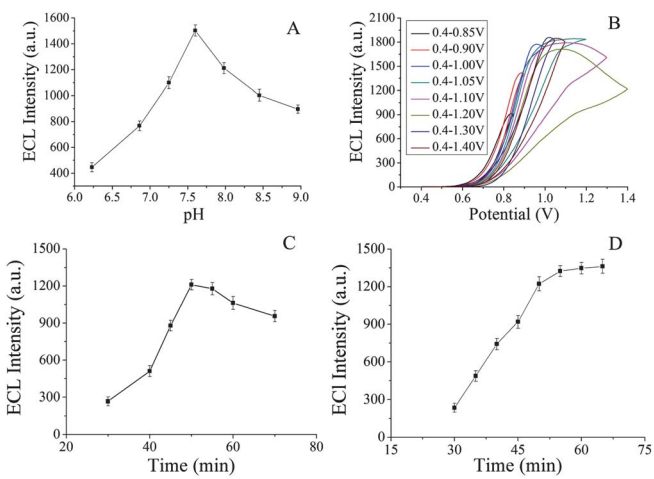

Fig. 3 Effect of pH (A), potential (B), T_1 (C), T_2 (D) on ECL intensity.

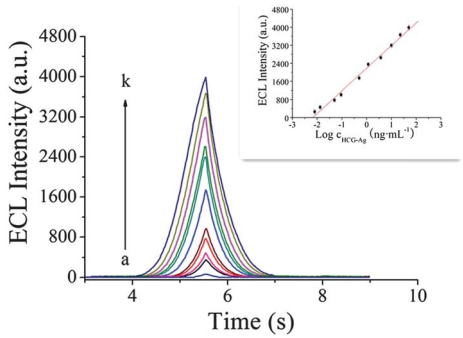

Fig. 4 ECL profiles of the ECL immunosensor in the presence of different concentrations of HCG-Ag in PBS containing 0.1M $K_2O_2S_8$. Inset: calibration curve for HCG-Ag determination. HCG-Ag determination (ng mL^{-1}): (a) 0, (b) 0.005, (c) 0.01, (d) 0.05, (e) 0.1, (f) 0.5, (g) 1.0, (h) 5.0, (i) 10.0, (j) 20.0, (k) 50.0.

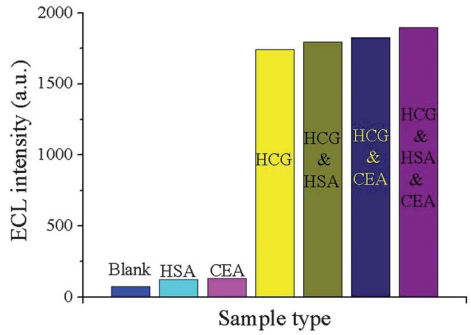

Fig. 5 Specificity of the immunosensor.

3.6. Reproducibility, specificity and stability of the immunosensor

Since reproducibility is a very important feature for an immunosensor, it was necessary to investigate this feature in the developed immunosensor. Reproducibility of the immunosensor for HCG-Ag was investigated with intraassay and interassay precision. Intraassay precision of the immunosensor was evaluated by assaying one level of HCG-Ag for six similar measurements. Interassay precision was estimated by determining one HCG-Ag level with six immunosensors. The intraassay and interassay variation coefficients obtained for 0.5 ng mL^{-1} HCG-Ag were 5.2% and 6.5% for the ECL assay (Table 1). Both intraassay and interassay applications demonstrated acceptable reproducibility. This could be ascribed to the simplicity of the label and the immunosensor preparing method.

To investigate the specificity of the immunosensor, 0.5 ng mL^{-1} HCG-Ag with 50 ng mL^{-1} carcinoembryonic antigen (CEA) and 50 ng mL^{-1} human serum albumin (HSA) were prepared, and then the ECL response of the mixture was detected. Compared with the ECL response of the immunosensor in 0.5 ng mL^{-1} pure HCG-Ag, no significant difference (RSD = 8.6%) was observed (Fig. 5), indicating that CEA and HSA could not cause the observable interference. The results suggest that the immunosensor displays good specificity to HCG-Ag and possesses high selectivity.

The stability of the proposed immunosensor was also examined by checking periodically its ECL intensity responses. When the immunosensor was not in use, it was stored in a refrigerator at 4 °C. After one week and two weeks, the ECL intensity of the immunosensor decreased to about 95% and 88% of its initial value, respectively. The slow decrease in the ECL intensity may be due to the gradual denaturing of CS and GA.

Table 1 The intraassay and interassay result of the proposed immunosensor

Items	Sample (ng mL^{-1})			RSD (%)
Intraassay	0.531	0.477	0.524	5.2
	0.482	0.525	0.478	
Interassay	0.527	0.469	0.535	6.5
	0.531	0.477	0.473	

3.7. Preliminary analysis of real samples

The feasibility of the immunosensor system for clinical applications was investigated by analyzing four samples prepared by the standard addition method. In comparison with the enzyme-linked immuno sorbent assay (ELISA) method, these serum samples were prepared by adding HCG-Ag of different concentrations to human serum samples.

Table 2 describes the correlation between the results obtained by the proposed ECL immunoassay and ELISA method. It obviously indicates that there is no significant difference between the two methods. Thus, the developed immunosensor could be applied to the clinical determination of HCG-Ag levels in human serum with satisfactory results.

3.8. Possible mechanism for the ECL behavior of CdTe QDs

ECL is a means of converting electrical energy to radiative energy. It involves the production of reactive intermediates from stable precursors at the surface of an electrode. These intermediates then react under a variety of conditions to form excited states that emit light.

From the ECL mechanism for CdS and CdSe QDs,[38–40] the ECL mechanism of CdTe QDs system could be inferred. The CdTe QDs immobilized on the Fe_3O_4/CS MNPs through immunoreaction were reduced to nanocrystalline species ($CdTe^{-\cdot}$), while the coreactant $S_2O_8^{2-}$ was reduced to the strong oxidant $SO_4^{-\cdot}$. $SO_4^{-\cdot}$ could react with the negatively charged $CdTe^{-\cdot}$ through electron transfer, which produced the excited

Table 2 Comparison of serum HCG-Ag levels determined using two methods

Serum samples	1	2	3	4
ECL immunosensor[a] (ng mL^{-1})	24.21	11.67	1.38	0.461
RSD (%)	4.35	3.98	5.14	4.71
Spiked (ng mL^{-1})	25.00	12.00	1.50	0.50
Recovery (%)	96.84	97.25	92.00	92.20
ELISA[a]	24.83	12.15	1.49	0.433
Relative error (%)	−2.49	−3.95	−7.38	6.47

[a] The average value of five successive determinations.

state (CdTe*) to emit light. The possible ECL mechanisms are described in Scheme 3, and the following eqn (1)–(4):

$$CdTe + e^- \rightarrow CdTe^{-\cdot} \quad (1)$$

$$S_2O_8^{2-} + e^- \rightarrow SO_4^{2-} + SO_4^{-\cdot} \quad (2)$$

$$CdTe^{-\cdot} + SO_4^{-\cdot} \rightarrow CdTe^* + SO_4^{2-} \quad (3)$$

$$CdTe^* \rightarrow CdTe + h\nu \quad (4)$$

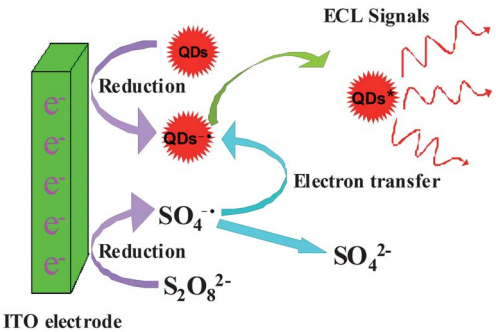

Scheme 3 ECL mechanisms of the CdTe QDs.

4. Conclusion

A novel ECL immunosensor has been developed by successfully combining Fe_3O_4/CS MNPs and QDs@PtRu with attractive features. The immunosensor could be conveniently aggregated and separated through a magnet, which is of great need in clinical fields, since the aggregation could be used to gather HCG-Ag for detection, even when the concentration is low. Besides, the QDs@PtRu exhibits good signal amplification, which makes it an ideal candidate for ECL immunosensing. The GA coated on the Fe_3O_4/CS MNPs enhances the ECL signal and its stability, and acts as a crosslinker to facilitate the ECL immunosensor. The novel immunosensor shows high sensitivity and selectivity, excellent stability, and good reproducibility, and thus has great potential for clinical detection of HCG-Ag. In particular, this approach presents a novel class of combining bifunctional nanomaterials with preferable Epropertiesies and excellent magnetism, which suggests considerable potential in a wide range of applications for bioassays.

Acknowledgements

This work was financially supported by the Natural Science Research Foundation of China (21175058), Natural Science Foundation of Shandong Province, China (ZR2011BQ019) and Technology Development Plan of Shandong Province, China (Grant No. 2011GGB01153).

Reference

1 K. Jain, *Nanomedicine*, 2006, **1**, 9–12.
2 D. P. Yang, S. H. Chen, P. Huang, X. S. Wang, W. Q. Jiang, O. Pandoli and D. X. Cui, *Green Chem.*, 2010, **12**, 2038–2042.
3 S. K. Sahoo, S. Parveen and J. J. Panda, *Nanomed.: Nanotechnol., Biol. Med.*, 2007, **3**, 20–31.
4 S. Mornet, S. Vasseur, F. Grasset and E. Duguet, *J. Mater. Chem.*, 2004, **14**, 2161–2175.
5 P. Juzenas, W. Chen, Y. Sun, M. Coelho, R. Generalov, N. Generalova and I. Christensen, *Adv. Drug Delivery Rev.*, 2008, **60**, 1600–1614.
6 D. Cui, Q. Li, P. Huang, K. Wang, Y. Kong, H. Zhang, X. You, R. He, H. Song, J. Wang, C. Bao, T. Asahi, F. Gao and T. Osaka, *Nano Biomed. Eng.*, 2010, **2**, 45–55.
7 D. Cui, B. Pan, H. Zhang, F. Gao, R. Wu, J. Wang, R. He and T. Asahi, *Anal. Chem.*, 2008, **80**, 7996–8001.
8 Y. Kong, J. Chen, F. Gao, W. Li, X. Xu, O. Pandoli, H. Yang, J. Ji and D. Cui, *Small*, 2010, **6**, 2367–2373.
9 S. F. Wang and Y. M. Tan, *Anal. Bioanal. Chem.*, 2007, **387**, 703–708.
10 J. S. Li, X. X. He, Z. Y. Wu, K. M. Wang, G. L. Shen and R. Q. Yu, *Anal. Chim. Acta*, 2003, **481**, 191–198.
11 M. Fuentes, C. Mateo, J. M. Guisan and R. Fernandez-Lafuente, *Biosens. Bioelectron.*, 2005, **20**, 1380–1387.
12 V. Mani, B. V. Chikkaveeraiah, V. Patel, J. S. Gutkind and J. F. Rusling, *ACS Nano*, 2009, **3**, 585–594.
13 A. Matthew, T. Cooper, Victoria and Singleton, *J. Mol. Recognit.*, 2007, **20**, 154–184.
14 J. P. Li and H. L. Gao, *Electroanalysis*, 2008, **20**, 881–887.
15 D. R. Deaver, *Nature*, 1995, **377**, 758–760.
16 M. Bruchez, M. Moronne, P. Gin, S. Weiss and A. P. Alivisatos, *Science*, 1998, **281**, 2013–2016.
17 L. L. Li, K. P. Liu, G. H. Yang, C. M. Wang, J. R. Zhang and J. J. Zhu, *Adv. Funct. Mater.*, 2011, **21**, 869–878.
18 P. Yang, A. Y. Zhang, H. S. Sun, F. T. Liu, Q. H. Jiang and X. Cheng, *J. Colloid Interface Sci.*, 2010, **345**, 222–227.
19 H. W. Gu, R. K. Zheng, X. X. Zhang and B. Xu, *J. Am. Chem. Soc.*, 2004, **126**, 5664–5665.
20 J. H. Gao, B. Zhang, Y. Gao, Y. Pan, X. X. Zhang and B. Xu, *J. Am. Chem. Soc.*, 2007, **129**, 11928–11935.
21 S. Zhang, F. Zheng, Z. Wu, G. Shen and R. Q. Yu, *Biosens. Bioelectron.*, 2008, **24**, 129–135.
22 M. Zhou, J. Roovers, G. P. Robertson and C. P. Grover, *Anal. Chem.*, 2003, **75**, 6708–6717.
23 K. A. Fahnrich, M. Pravda and G. G. Guilbault, *Talanta*, 2001, **54**, 531–559.
24 L. J. Hua, H. Y. Han and H. B. Chen, *Electrochim. Acta*, 2009, **54**, 1389–1394.
25 Z. P. Chen, Z. F. Peng, Y. Luo, B. Qu, J. H. Jiang, X. B. Zhang, G. L. Shen and R. Q. Yu, *Biosens. Bioelectron.*, 2007, **23**, 485–491.
26 W. C. Mak, K. Y. Cheung, D. Trau, A. Warsinke, F. Scheller and R. Renneberg, *Anal. Chem.*, 2005, **77**, 2835–2841.
27 N. Dolinnaya, M. Jan, A. Kawde, T. Oretskaya, V. Tashlitsky and J. Wang, *Electroanalysis*, 2006, **18**, 399–404.
28 X. Liang, J. J. Xiao, B. H. Chen and Y. D. Li, *Inorg. Chem.*, 2010, **49**, 8188–8190.
29 Y. F. Shi, B. K. Guo, S. A. Corr, Q. H Shi, Y. S. Hu, K. R. Heier, L. Q. Chen, R. Seshadri and G. D. Stucky, *Nano Lett.*, 2009, **9**, 4215–4220.
30 Y. K. Peng, C. W. Lai, C. L. Liu, H. C. Chen, Y. H. Hsiao, W. L. Liu, K. C. Tang, Y. Chi, J. K. Hsiao, K. E. Lim, H. E. Liao, J. J. Shyue and P. T. Chou, *ACS Nano*, 2011, **5**, 4177–4187.
31 J. H. Pan, S. Y. Chai, C. M. Lee, S. E. Park and W. I. Lee, *J. Phys. Chem. C*, 2007, **111**, 5582–5587.
32 X. Xue, X. Z. Zhou and G. J. Zhang, *Guangzhou Chem (China)*, 2010, **38**, 81–84.
33 C. X. Xu, L. Wang, M. L. Mu and Y. Ding, *Langmuir*, 2010, **26**, 7437–7443.
34 N. Gaponik, D. V. Talapin, A. L. Rogach, K. Hoppe, E. V. Shevchenko, A. Kornowski, A. Eychmüller and H. Weller, *J. Phys. Chem. B*, 2002, **106**, 7177–7185.
35 F. Novio, P. G. Duarte, A. Lledos and R. M. Balleste, *Chem.–Eur. J.*, 2007, **13**, 1047–1063.
36 H. Sellers, *Surf. Sci.*, 1992, **264**, 177–184.
37 K. Z. Liu, L. L. Shi, M. S. Jin and Z. H. Suo, *J. Mol. Catal. (China)*, 2009, **23**, 436–441.
38 D. J. Lin, J. Wu, F. Yan, S. Y. Deng and H. X. Ju, *Anal. Chem.*, 2011, **83**, 5214–5221.
39 G. F. Jie, J. J. Zhang, D. C. Wang, C. Cheng, H. Y. Chen and J. J. Zhu, *Anal. Chem.*, 2008, **80**, 4033–4039.
40 G. F. Jie, H. P. Huang, X. L. Sun and J. J. Zhu, *Biosens. Bioelectron.*, 2008, **23**, 1896–1899.

